

4.1 Extending the Walker code

Changing the code so that the second boundary condition is that of a specified temperature on the back face of a slab, we were able to move away from the semi-infinite solid limitation. The heat fluxes at the back face and the surface are obviously dependent on the temperature gradient at that position, which in turn is dependent on the measured temperature there. The boundary condition at the thermocouple at the back is given below. “back” is the temperature at the back face at a specific point in time. “for” is twice the Fourier number, $\alpha t/L^2$. a, b, c, and d are the coefficients of the tridiagonal matrix, used to solve for the temperature distribution through the solid at a given point in time. It is important to note that the changes were made to the conduction solver and not to the inverse method itself.

```
C      Interior boundary at a specific temperature
      a(nx) = - 0.5 * for
      b(nx) = 1 + for
      c(nx) = 0
      r(nx) = (0.5*for*back) + t(nx-1)
```

The use of this boundary condition ensures that the slope of the temperature curve is not zero at the back, as is the case with the semi-infinite approach [11]. To be able to do this, all the subroutines need to have an extra variable, which is the temperature at the back face. The penetration depth was also set at 0.025m, for this specific blade in the cascade tunnel. The user can change this value at any time to any value. These tests will be described below. This value can easily be changed for different situations. The output of this program is given in five columns. These are the time, the guessed flux, the surface temperature, the temperature at the back and then the heat flux at the surface. Other changes were made to save the values of the temperatures at the back and the subroutines were changed in such a way that the back face temperature was incorporated there as well. For example:

```
32      ct = 1
      READ(10,*,END=31) tm(ct), q0(ct), y(ct), bft(ct)
      ct = ct + 1
      GOTO 32
```

In this case, t_m is the time, q_0 is the guessed flux, y is the surface temperature and bft is the back face temperature.

```
CALL imp2(bft(tpos),nx,t,qi(0),qi(1),dx,dt)
```

Apart from these changes, a few other minor changes were made. See Appendix D for the entire code and the modifications made in it. As evident in Chapter 3, the temperature profiles generated by the original code all coincide at the back. This is because the code uses a semi-infinite solid approach for the generation of these profiles. The modified code reads the temperature at the back and in each iteration this temperature is used as the temperature on the back face. The back face temperature changes throughout the run and does not stay equal to the original temperature of the blade.

4.2 Noise decrease.

In Chapter 2, an investigation was made to see what the effect of noise on the temperature signal is when using the Cook-Felderman technique. The Cook-Felderman technique was responsible for a great deal of amplification of this noise when converted to heat flux. A comparison will now be made between the Cook-Felderman technique and the inverse approach, by using the same temperature signal with superimposed sinusoidal noise. In the figure below, the temperature signal is shown with the imposed noise on. This signal was generated in the same way the signals in Chapter 2 were generated.

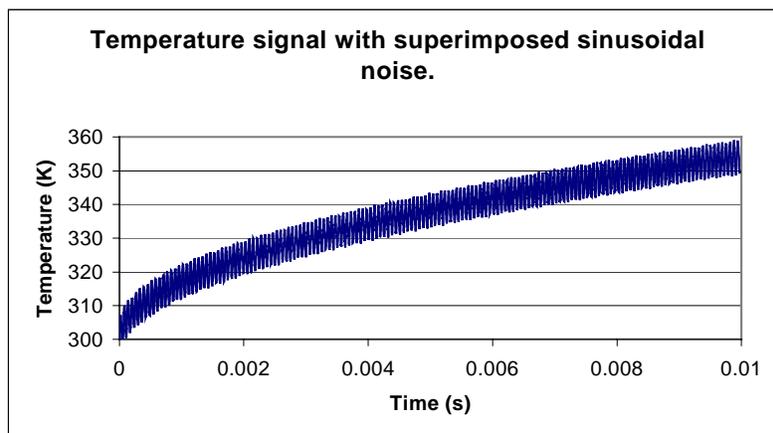


Figure 4.1 Input temperature signal with superimposed noise with frequency 16 kHz.

Using the signal in *figure 4.1* the Cook-Felderman technique generates a heat flux signal which is very noisy. The heat flux signal is shown in *figure 4.2*.

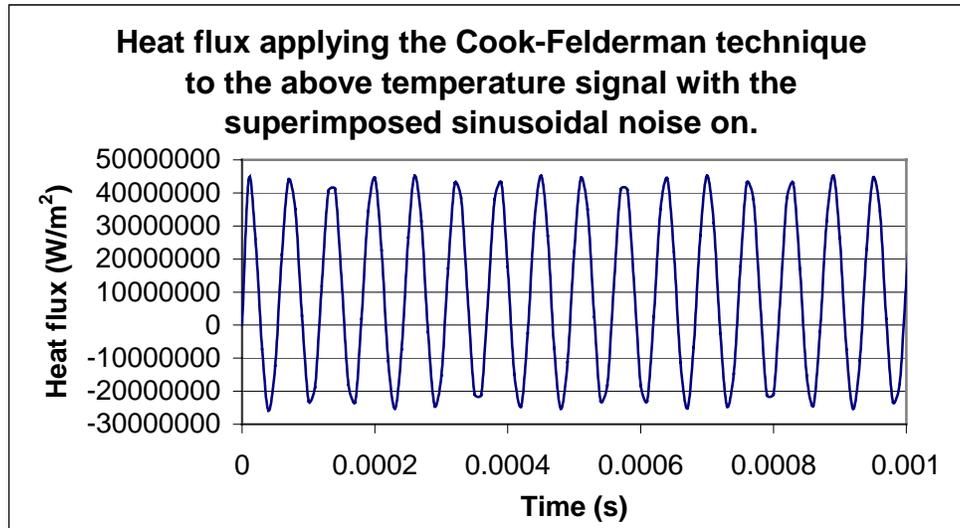


Figure 4.2 Predicted heat flux using the Cook-Felderman technique and the temperature in figure 4.1 as input.

Although the value used in theory of 10 MW/m^2 is much larger than the measured values, which were something in the region of 10 W , the effect of the noise should be nominally linearly with the heat flux. At Virginia Tech tests could only be conducted for low heat fluxes.

The true flux in this case is 10 MW/m^2 . It's clear that the average of this signal is 10 MW/m^2 , but the oscillation of the flux around this mean, is very large. The amplitude is thus unacceptably high. As an improvement on this, a decision was made to use the inverse method of obtaining the heat transfer from the surface temperature measurements. This method proves to be much more stable in the sense that the heat flux obtained by using the inverse method does not suffer the loss of efficiency due to the instability induced by the Cook-Felderman technique.

In *figure 4.3* the heat flux is shown when using the inverse method. This figure reveals the fact that the inverse approach does not amplify the noise imposed on the temperature signal as much as is the case with the Cook-Felderman method. If a comparison is made between the amplitude of noise imposed on the heat flux for the two methods, the result is as follows:

$$\frac{ABS(Amplitude)}{True / Mean_value} * 100\% = \frac{ABS(10 - 45)}{10} * 100\% = 350\% \quad (4.1)$$

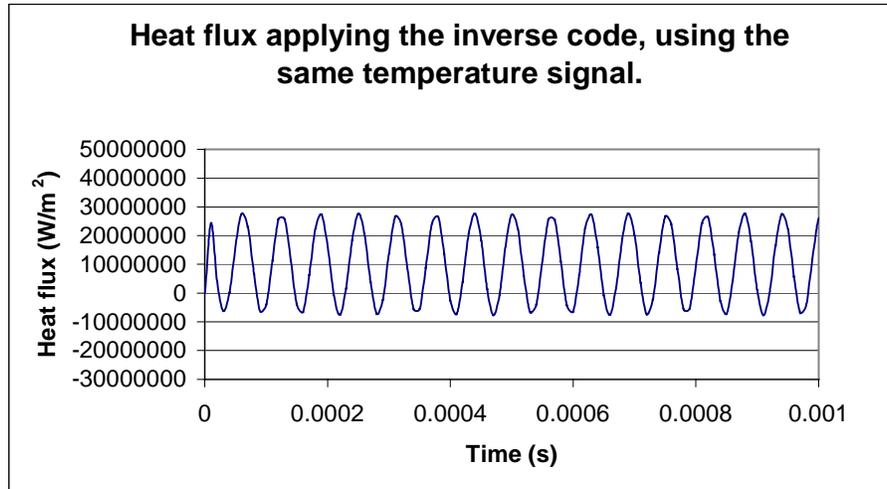


Figure 4.3 Predicted heat flux using the inverse method and the temperature in figure 4.1 as input.

If the same evaluation is done using the inverse approach the following result is found:

$$\frac{ABS(Amplitude)}{True / Mean_value} * 100\% = \frac{ABS(10 - 27)}{10} * 100\% = 170\% \quad (4.2)$$

Repeating this same evaluation with evenly distributed, random noise the following results are obtained. The results are very similar to those obtained with the superimposed sinusoidal noise.

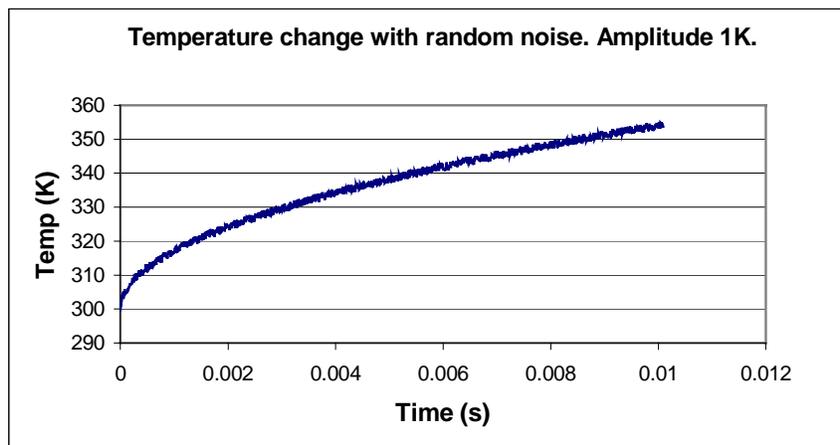


Figure 4.4 Created temperature signal with superimposed random noise.

As seen in the above figure the noise amplitude is much smaller than the previous theoretical analysis in *figure 4.1*. This was done because the amplitude of 5K is somewhat over conservative, but was used to show the basic effect of the noise on the eventual heat flux signal. In the next figure, *figure 4.5*, the heat flux was calculated with the Cook-Felderman method.

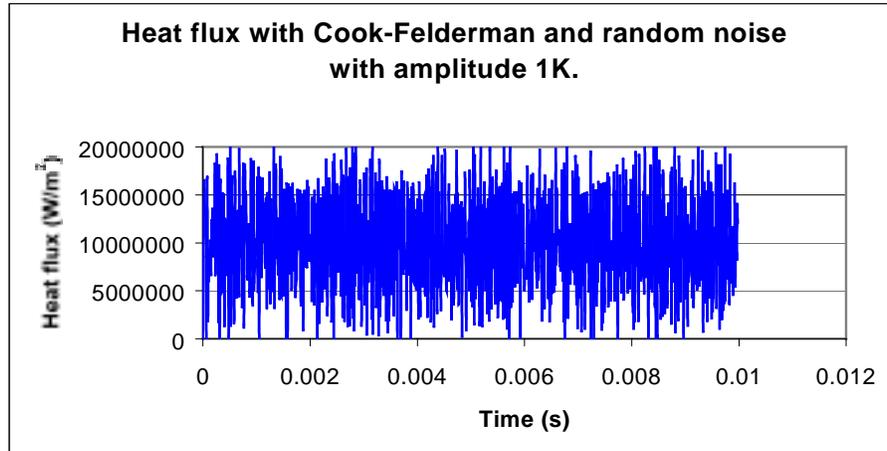


Figure 4.5 The flux for the temperature in figure 4.4 using Cook-Felderman.

If the same calculation is done with the inverse method, the heat flux signal looks much better. The frequency as well as the amplitude of the noise is less, than that predicted by the simple superposition of the sinusoidal noise on the temperature signal. See *figure 4.6* for the flux calculated with the inverse method.

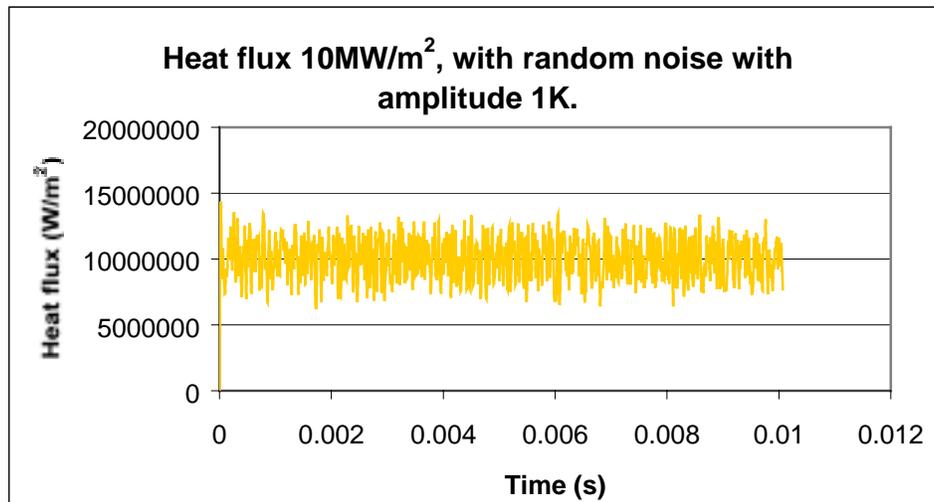


Figure 4.6 The flux for the temperature in figure 4.4 using the inverse approach.

$$\frac{ABS(Amplitude)}{True / Mean_value} * 100\% = \frac{ABS(10 - 12.5)}{10} * 100\% = 25\% \quad (4.3)$$

In comparison with the values in eq. 4.1 and 4.2 this value of 25% is a good improvement on the noise amplitude in the results. It is, therefore, clear that an increase in the frequency, as well as an increase in the amplitude of the noise on the temperature signal, will affect the output negatively. The inverse method suppresses the amplitude of the noise through the introduction of relaxation and bias in the code.

4.3. Experimental test case

By using some data obtained from the Cascade Tunnel at Virginia Tech, a few case studies were made. The objective of these case studies were:

- to remove the semi-infinite solid approach and make the application of the method for estimating heat flux more universal. This includes the modification to the code to be able to utilize a time dependent internal boundary condition, and not only a specified constant temperature.
- to compare the newly developed results to those from a commercial heat flux gage.

4.4 Experimental set-up

The basic layout of the test facilities can be seen in *figure 4.7*.

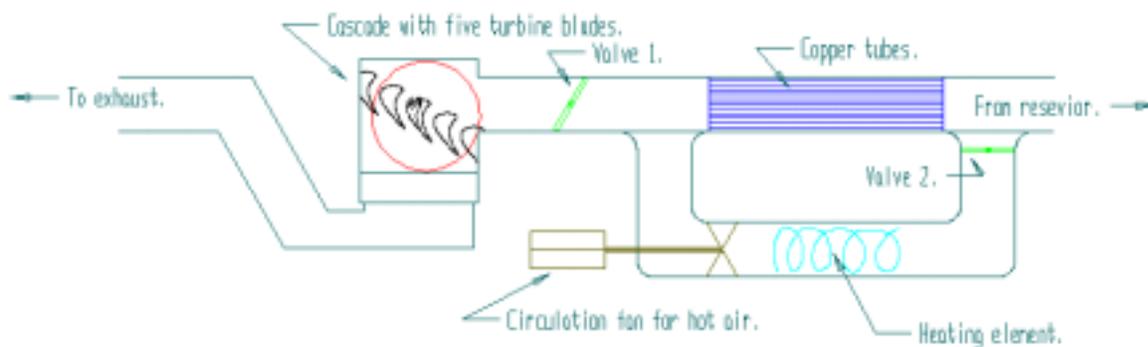


Figure 4.7 Virginia Tech cascade tunnel.

See this web-page for further detail on these facilities:

<http://www.aoe.vt.edu/aoe/physical/cascade.html>

The heating element warms the air while it is circulated through the loop system. Valve 1 is closed and valve 2 is opened. Heat is then transferred to the copper tubes by means of convection. The instant before the tunnel is run, valve 1 is opened and valve 2 is closed. The air from the reservoir is then heated as it runs through the hot copper tubes. This hot air then runs through the cascade and out the exhaust. Photos of the blade in the cascade tunnel are shown in *figure 4.8* and *4.9*. See Appendix C for more photos of the cascade tunnel facilities.



Figure 4.8 Instrumented blades in the cascade tunnel.



Figure 4.9 The blades in the tunnel with the film-cooling-air pipe.

A 3-D view of the blade is shown in figure 4.10.

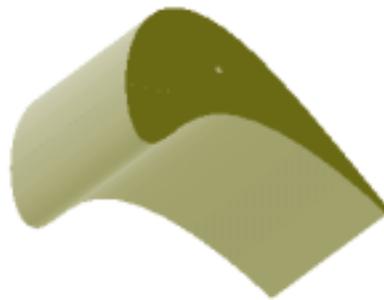


Figure 4.10 A 3-D view of the test blade.

In *figure 4.11* the schematic layout of the two thermocouples installed in the blade is shown.

The distance between the two thermocouples is 25mm. Wires to both of these gages run through a hole in the side of the blade and out through the wall of the cascade tunnel.

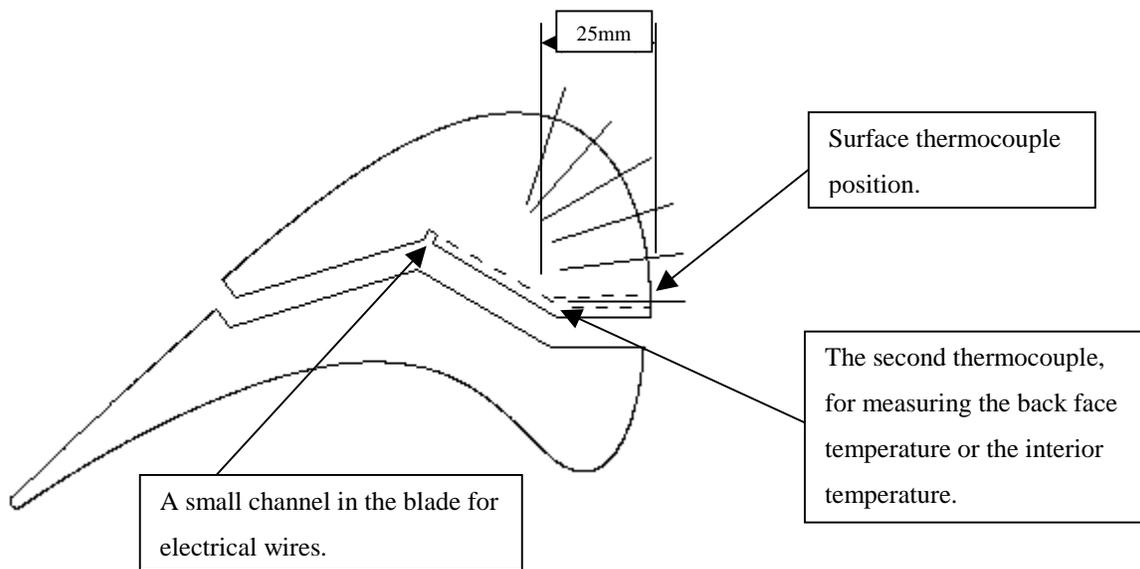


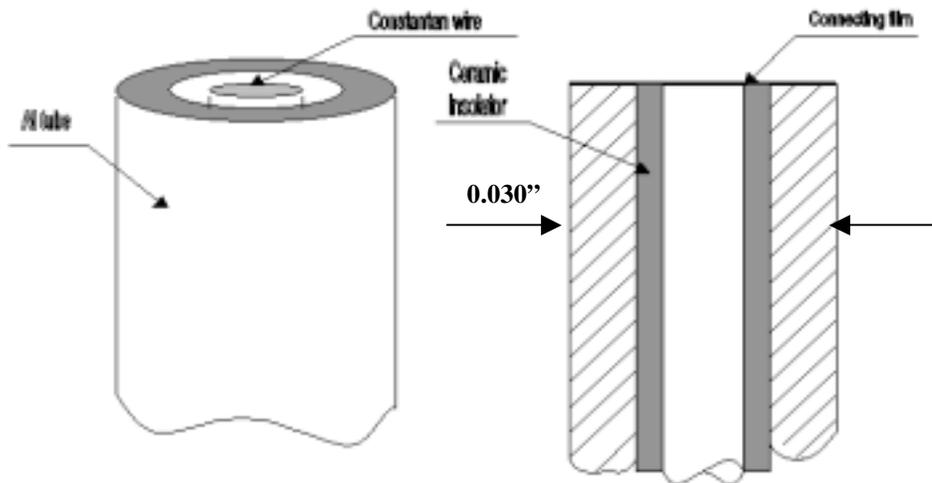
Figure 4.11 The blade with the two thermocouple positions.

There were two aluminum blades used in these experiments. The first blade was fully instrumented with six thermocouples, six HFS heat flux gages [26] and six Kulite pressure sensors. The thermocouples in this blade were Copper/Constantan, also known as type K. Another similar blade was used but with only one of each of the gages installed at the surface (see *figure 4.7.*) In this blade, another thermocouple was installed in addition to the type K thermocouples. This thermocouple was custom made by the “Medtherm” company. This thermocouple is not a conventional one, because it’s made from aluminum (Al) and Constantan. The reason why aluminum was used was to match the thermophysical properties of the aluminum blade that will carry the thermocouple in one test application, as closely as possible. This will ensure that the heat flux through the thermocouple itself will be as close as practically achievable to the actual flux through the body. The blade is made of 6061 aluminum alloy. The thermocouple is made of 3003 aluminum. The thermophysical properties of these alloys are given in *Table 4.1.*

Table 4.1 Comparison of properties between the model blade and the thermocouple.

	Blade	Thermocouple
Aluminum Alloy	6061	3003
Density kg/m ³	2700	2720
Conductivity W/m.K	155 - 180	162
Specific heat J/kg.K	896	893

The basic concept of the thermocouple is visible in *Figure 4.12*.

**Figure 4.12 Al-Constantan thermocouple.**

As seen from *Figure 4.12*, the thermocouple is made from a small Al tube on the outside and a very thin constantan wire on the inside. A thin ceramic insulator tube (Alumina) then separates the two conductors. The electrical connection on top of the thermocouple, is made by depositing a thin film ($\approx 1\mu\text{m}$) of Al on the top. The thinner the connecting layer, the faster the response time of the thermocouple. This thermocouple will be used to measure the surface temperature. The distance between the surface and back face thermocouples is approximately 25mm. In the code this distance is divided into 100 grid points. This gives a fairly fine grid, but is also a convenient number. The spacing is 0.25mm. If this number is increased, the time to convergence increases dramatically.

The temperature inside the blade was measured with a type-K thermocouple glued to the metal with a metal epoxy.

Conventional thermocouples usually make use of an electronic ice bath built into the computer. In this case it was not possible because of the unusual thermocouple metal pair used, therefore a real ice bath was used to create the reference temperature of 0°C .

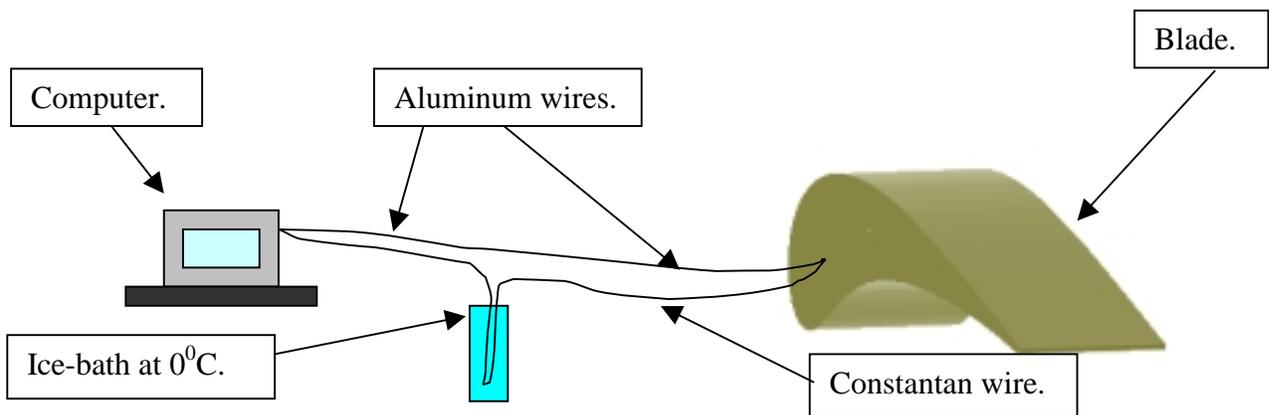


Figure 4.13 Experimental set-up.

Figure 4.13 shows the basic ice-bath set-up. The voltage measured by the computer is directly proportional to the difference in the temperature between the blade and the ice-bath. The ice-bath is at 0°C , which makes it a very appropriate reference temperature. The frequency at which data was taken was 100Hz. This particular value was chosen because all the other measurements were done at this frequency, and the same LabView program was used to accumulate all the data from the heat flux gages, pressure gages, thermocouples etc. The calibration factor used in the domain of output voltage from the thermocouple was $39.6\mu\text{V}/^{\circ}\text{C}$. (Supplied by Medtherm)

In *figure 4.14* below, the measured temperature on the surface as given by our aluminum thermocouple as well as the measured temperature at the specified depth below the surface is given as a function of time.

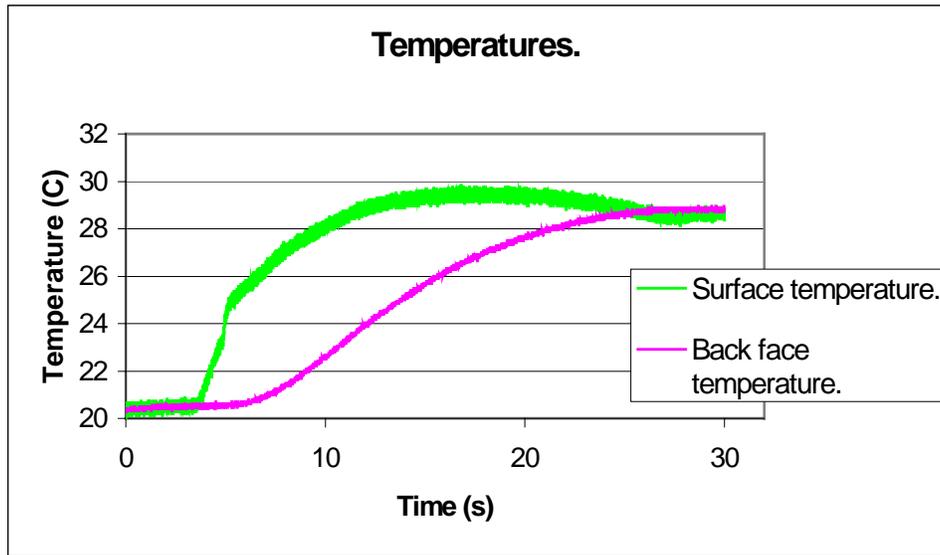


Figure 4.14 Measured surface and internal temperature.

Keeping this graph in mind and using the original Walker code to calculate the heat flux through the wall and into the object, the temperature profile at a specific depth beneath the surface can be calculated assuming a semi-infinite body. If this depth is equal to the distance to the back face, the temperature profile should correspond to the measured profile at the back. This is not the case beyond about 12 seconds, and the deviation can be seen in *figure 4.15*. This discrepancy is caused by the fact that the original code uses a semi-infinite solid approach.

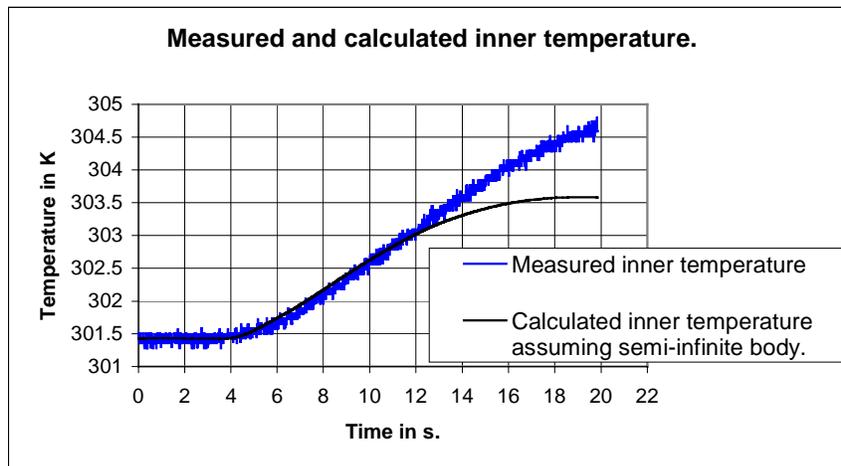


Figure 4.15 Difference between the measured and calculated temperature, using the original code that assumes semi-infinite body.

The HFS heat flux gage is also able to measure a temperature, using a platinum resistance thermometer. The electric resistance changes with temperature, and the voltage output can then be related to the temperature on the surface. This temperature, the RTS temperature, is graphed in *figure 4.16*. The HFS gage consists of a number of thermocouples connected in series across a thin thermal resistance layer [14]. This is done to amplify the voltage output from the gage.

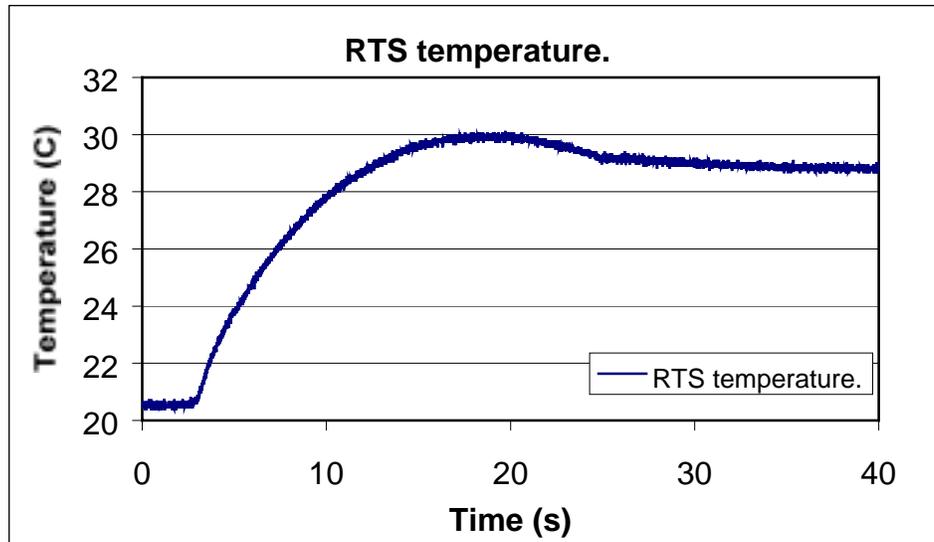


Figure 4.16 RTS surface temperature.

When comparing the RTS and the aluminum thermocouple temperatures, there is a slight difference as shown in *figure 4.17*. A possible error might be a delay in the RTS temperature measured, because of the larger thermal mass associated with the heat flux gage. The sensitivity of the Medtherm thermocouple is very good. This is achieved with the thin connecting layer on top. The response times are also very fast, and claims by Medtherm are in the order of 1 μ s. This is faster than is possible with most of the other conventional heat flux gages. These thermocouples have been used in the past for the measurement of temperature in gun barrels. Under these extreme conditions, Medtherm claims that they performed well [23].

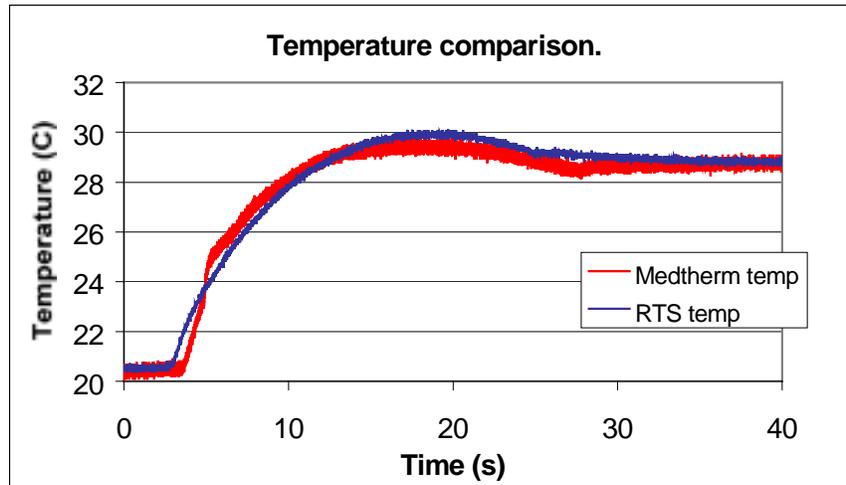


Figure 4.17 Comparison of the RTS and coaxial surface temperatures.

The heat flux measured by the HFS gage is presented in *figure 4.18*, below. In the figure, data acquisition started at time zero. The moment heated air started to flow, (the tunnel is being turned on) the curve shows measurable values of heat flux after approximately 3 seconds. The maximum of this curve is approximately 5 W/cm^2 , and this maximum is at 4.2s.

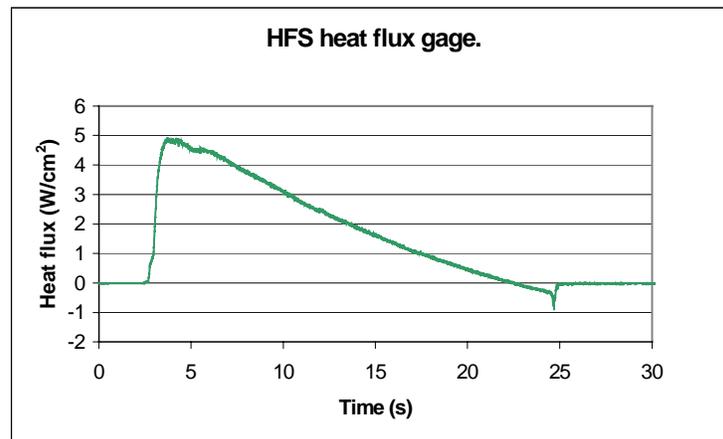


Figure 4.18 HFS heat flux.

First, the heat flux obtained by using the measured temperature profile in *figure 4.18* in a simple implicit finite difference method (Class 2) was used to see if the answers are in the same range. This is a normal finite difference method, using the two measured temperatures (the coaxial thermocouple and the type-K thermocouple temperatures) as the boundary conditions. In this and

the next approaches, the time step and the spacing were the same as in all the other cases. $\Delta x = 0.25\text{mm}$ and $\Delta t = 0.01\text{s}$. Due to the noise that gets amplified, an answer is fairly difficult to achieve. In the graph an average was calculated for the noisy heat flux – the average of every ten points of a total of 30000 points were calculated. This average gives a much more reasonable answer.

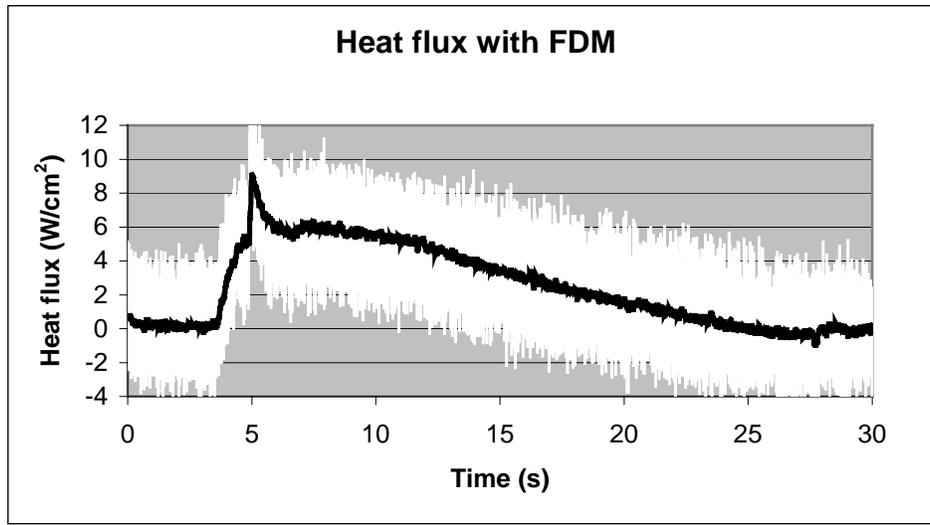


Figure 4.19 Heat flux predicted with a simple implicit finite difference (Class 2) technique.

The problem with this approach is the effects of noise and this method is fairly difficult, because the independence of the result as a function of decreasing grid spacing converges very slowly. However, this graph is a indication of the answer that one can expect. The sharp peak in the heat flux is due to the sharp increase in the temperature at this point measured by the Medtherm thermocouple. If this initial spike is ignored, for the moment, the maximum value of the flux in this case, is on the order of 6 W/cm^2 , which can be compared to the HFS maximum of 5 W/cm^2 . This does not mean that the spike can be ignored when we look at the global picture. The HFS gage might smear this spike, because of its larger “footprint.”

Now, using the extended version of the Walker code, we get an answer very similar to the one in the above figure as shown in *figure 4.20*. The most obvious characteristic of *figure 4.20* is the fact that the noise is much less than that produced by the finite difference method in *figure 4.19*.

The results are qualitatively similar. The maximum is approximately 6 W/cm^2 compared to the value of 5 W/cm^2 from the HFS gage.

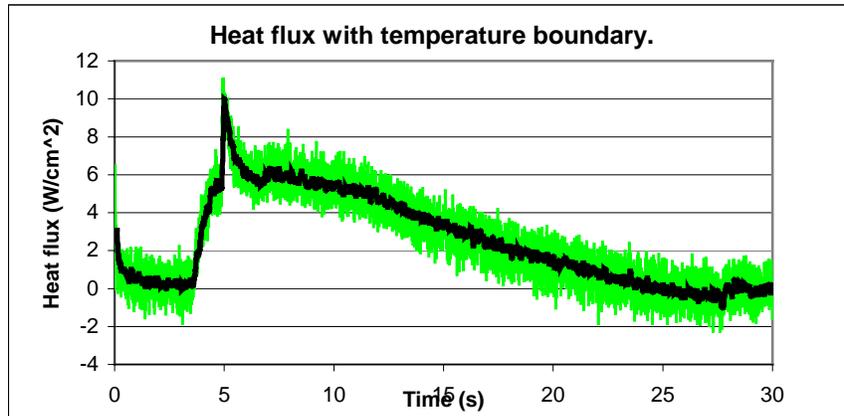


Figure 4.20 Predicted heat flux from the extended inverse code.

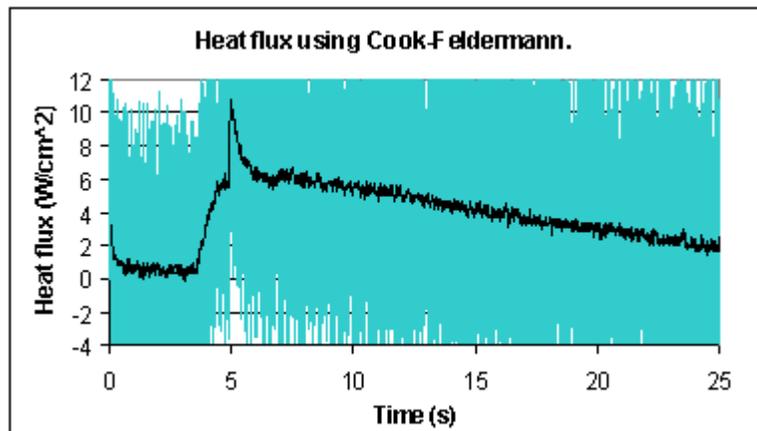


Figure 4.21 Same flux as in figure 4.20 but with the Cook-Felderman technique.

Last, using the same surface temperature from the Medtherm thermocouple, but this time the simpler Cook-Felderman technique, the predicted flux in *figure 4.21* is the outcome. The blue signal is the original and the black is an average. If one looks closely, the flux at 20s, in *figure 4.20*, is lower compared to that obtained in *figure 4.21*. This is because the internal temperature is rising (seen in *figure 4.14*), therefore the flux will be less than in the semi-infinite solid case as assumed in the Cook-Felderman method. In the semi-infinite solid case, the temperature in the middle of the blade is assumed to be constant. In reality this is not the case. The temperature does rise, and the slope of the temperature profile will be slightly less, causing the flux to be less as well.

4.5 Conclusions

Looking at all the graphs in this chapter, it is clear that the flux estimated by the new code is somewhat higher than that suggested by the calibrated HFS heat flux gages. On the other hand the flux obtained from the RTS temperature from the HFS gage, through the Cook-Felderman scheme, gives a very similar numerical value to the flux up until the time where the semi-infinite assumption in the Cook-Felderman method is no longer valid. This is due to the fact that the temperature profiles are very similar. The HFS gages are calibrated to give a certain voltage for a certain heat flux. The calibration is, however, subject to errors.

A potential cause for the discrepancies is that the heat flux is assumed to be 1-D in all cases. It is important to keep in mind that 2-D heat flow might be of such a great effect that the flux obtained numerically through the evaluation of the surface temperatures, is not reliable. In the next chapter, 2-D effects will be evaluated to see whether they are of substantial importance or not.



DEPARTMENT OF AEROSPACE AND OCEAN ENGINEERING

Transonic Cascade Wind Tunnel

The Virginia Tech Transonic Cascade Wind Tunnel is a blow down transonic facility capable of a twenty second run time. An overall layout is given in Figure X, and a photo is shown in Figure Y. The air supply is pressurized by a four-stage Ingersoll-Rand compressor and stored in large outdoor tanks. The maximum tank pressure used for transonic tests is about 1725 kPa (250 psig).

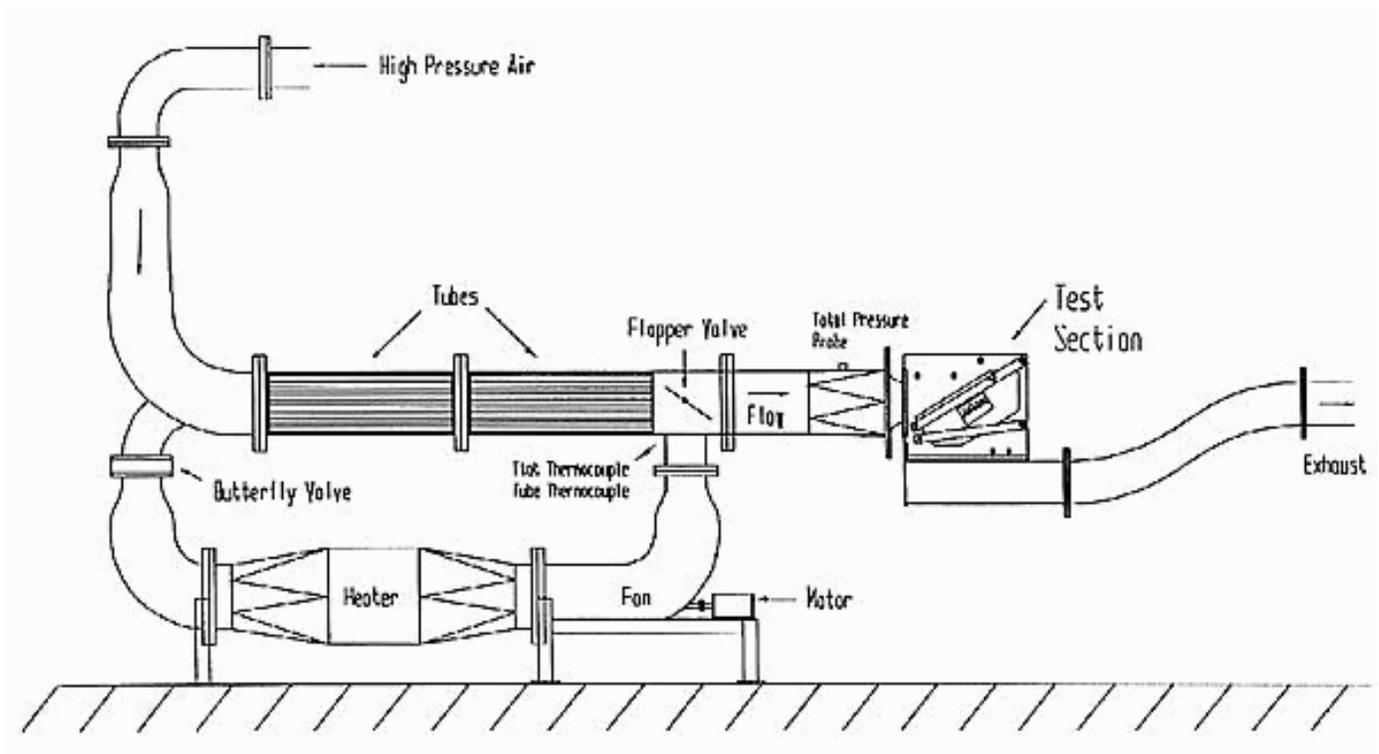


Figure X. Transonic Cascade Wind Tunnel Layout

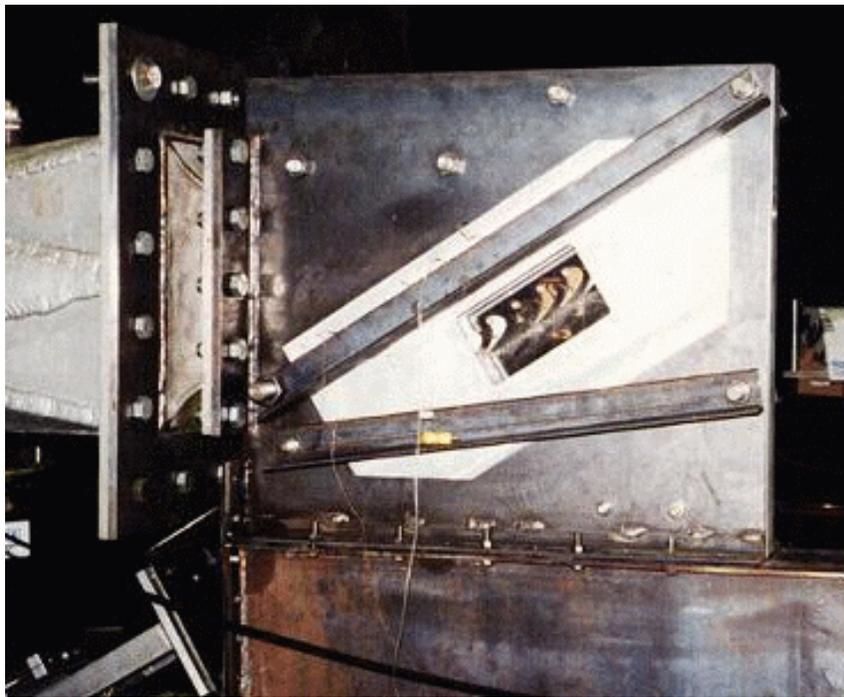


Figure Y. Photograph of the Cascade Wind Tunnel Test Section

During a run, the upstream total pressure is held constant by varying the opening of a butterfly valve controlled by a computerized feedback circuit. There is also a safety valve upstream of the control valve to start and stop the tunnel. The test section area is 37.3 cm high, and is designed for blades with an outlet angle of approximately 70 degrees. The blade isentropic exit Mach number is varied by changing the upstream total pressure; the usual range for exit Mach number is 0.7 to 1.35. The throat Reynolds number for typical tests is 340,000.

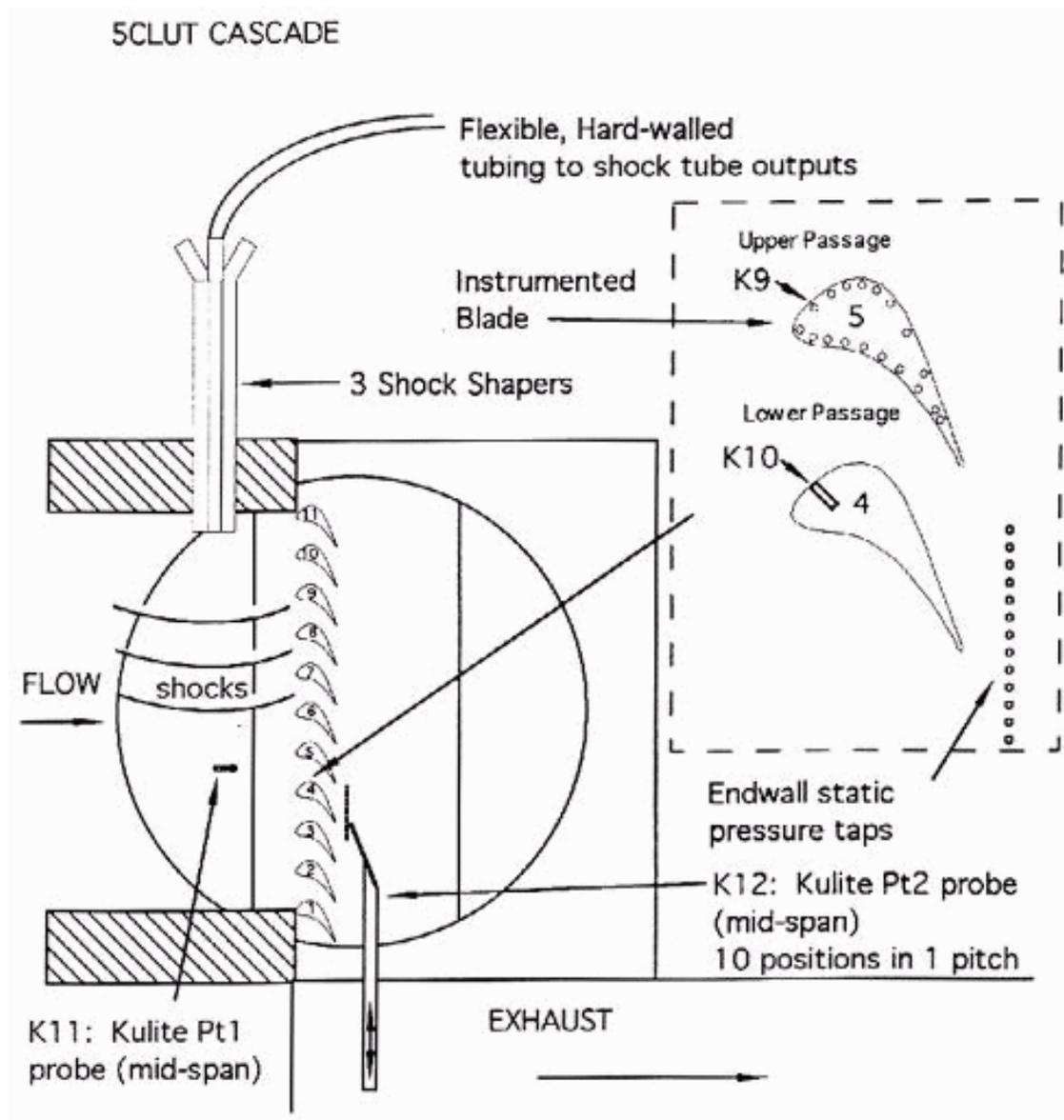


Figure Z. Typical Test Section Diagram

Figure Z is a diagram of the test section. The tunnel mean flow is left to right on the figure, and is turned through 68 degrees by the blade passages, which act as the tunnel throat. Upstream of the blades, the bundle of three shock shapers protrudes from the test section top block; the shocks propagate down from the shaper exit to the bottom of the test section. The high-response total pressure probe for downstream surveys is also shown on the figure, pointing into the cascade exit flow. The probe moves up and down in line with wall static pressure taps. No tailboard is used downstream of the cascade, which means that a free shear layer forms between the exit plane of the blades and the test section back wall. Note also the upstream total pressure probe, which is fixed at mid-pitch of the “Lower” passage.

Back to [Facilities](#)

Back to [High-Speed Flow Research](#)

Send comments and suggestions to
webmaster@aoe.vt.edu

Copyright © 1996 AOE Dept., Virginia Tech All rights reserved world wide